membranes

MDPI

Article

Gas Permeation Properties of High-Silica CHA-Type Zeolite Membrane

Yasuhisa Hasegawa *, Chie Abe, Mayumi Natsui and Ayumi Ikeda

Research Institute of Chemical Process Technology, National Institute of Advanced Industrial Science and Technology, 4-2-1 Nigatake, Sendai 983-8551, Japan; abe-chie@aist.go.jp (C.A.); natsui-mayumi@aist.go.jp (M.N.); a-ikeda@aist.go.jp (A.I.)

* Correspondence: yasuhisa-hasegawa@aist.go.jp

Abstract: The polycrystalline CHA-type zeolite layer with Si/Al = 18 was formed on the porous α-Al_2O_3 tube in this study, and the gas permeation properties were determined using single-component H_2, CO_2, N_2, CH_4, n-C_4H_{10}, and SF_6 at 303–473 K. The membrane showed permeation behavior, wherein the permeance reduced with the molecular size, attributed to the effect of molecular sieving. The separation performances were also determined using the equimolar mixtures of N_2–SF_6, CO_2–N_2, and CO_2–CH_4. As a result, the N_2/SF_6 and CO_2/CH_4 selectivities were as high as 710 and 240, respectively. However, the CO_2/N_2 selectivity was only 25. These results propose that the high-silica CHA-type zeolite membrane is suitable for the separation of CO_2 from CH_4 by the effect of molecular sieving.

Keywords: zeolite membrane; CHA-type zeolite; gas permeation; CO_2 separation

Citation: Hasegawa, Y.; Abe, C.; Natsui, M.; Ikeda, A. Gas Permeation Properties of High-Silica CHA-Type Zeolite Membrane. *Membranes* **2021**, *11*, 249. https://doi.org/10.3390/membranes11040249

Academic Editor: Tomohiro Kyotani

Received: 11 March 2021
Accepted: 26 March 2021
Published: 30 March 2021

1. Introduction

Zeolites are microporous aluminosilicate compounds, and they have been attracted much attention as the potential material for membranes. Zeolite membranes have been studied since the 1990s, and the MFI-type zeolite membranes were formed on the substrates by deposition and intergrowth of crystallites, which were nucleated in synthesis mixtures [1–10]. Geus et al. [1] prepared MFI-type zeolite membranes on several kinds of substrates and determined gas permeation properties through the membranes. Sano et al. [2] investigated MFI-type zeolite membranes by a hydrothermal process on porous stainless-steel and alumina substrates and applied them to the separation of water/alcohol mixtures. The permeation and separation properties were also studied by several groups [11–17]. Moulijn and coworkers [11–14] estimated the permeation properties through the MFI-type zeolite membranes using a Maxwell–Stefan formulation containing the gas adsorption on zeolites and the diffusion inside the membrane. Morooka and coworkers [15,16] proposed an adsorption–diffusion model to discuss the effect of CO_2 adsorption on zeolite and diffusion in the membrane for CO_2 separation using Y-type zeolite membranes. Some kinds of zeolite membranes are available for the dehydration of many kinds of organic solvents in industries [18–22].

These mechanism studies have established that DDR-, CHA-, and AEI-type zeolite has favorable characteristics for the membrane material, such as small micropore diameter, large micropore volume, and the composition variability [23]. These features correspond to the permeation and separation performances and the acid and thermal stabilities of the membrane [24]. Tomita et al. developed the DDR-type zeolite membrane by the secondary growth of seeded crystals [20], and the several gas permeation properties were determined [25]. In particular, the CO_2/CH_4 selectivity was as high as 2000 below 250 K. However, the selectivity decreased to 220 around 300 K. Noble and coworkers investigated CHA-type silica-aluminophosphate zeolite (SAPO-34) membranes [26–30], and the separation performances were determined for CO_2–CH_4, CO_2–N_2, Kr–Xe, and N_2–CH_4 mixtures. The CO_2/CH_4 selectivity was 171 at 295 K [28]. Some high-silica

CHA-type zeolite membranes with no phosphates were developed, and the dehydration and CO_2 separation performances were determined [31,32]. Sato et al. developed the commercially available CHA-type zeolite membranes with Si/Al = 7, and the dehydration performances were determined for *N*-methyl-2-pyrrolidone (NMP) [31]. For a 50 wt % NMP solution at 403 K, the permeation flux and separation factor were 36 kg m^{-2} h^{-1} and 1100, respectively. Imasaka et al. developed high-silica CHA-type zeolite membranes with Si/Al = 23, and they applied them to the CO_2 separation [32]. The membrane showed the high CO_2 permeance (1.5×10^{-6} mol m^{-2} s^{-1} Pa^{-1}) and CO_2/CH_4 selectivity (115) at 313 K. AEI-type zeolite is one of the aluminophosphate-type zeolites and contains no exchangeable cations. Since the crystal structure is similar to CHA-type zeolite, the identical CO_2/CH_4 selectivities were obtained [33–35].

Recently, we developed the rapid preparation technique for high-silica CHA-type zeolite membranes using the structure conversion of Y-type zeolite [36–38]. The influence of preparation conditions on the separation performances were studied, and the high reproducible procedures were determined [37]. The dehydration performances were determined for several organic solutions in our previous report [38]. However, the gas permeation and separation performances have not been determined. In this study, the gas permeation properties were determined using single-component H_2, CO_2, N_2, CH_4, *n*-C_4H_{10}, and SF_6 at 303–473 K. The gas separation tests were also examined for binary mixtures of N_2-SF_6, CO_2-N_2, and CO_2-CH_4 at 303–473 K. Furthermore, the gas permeation and separation mechanisms of the CHA-type zeolite membrane were discussed in this paper.

2. Materials and Methods

2.1. Membrane Preparation

A high-silica CHA-type zeolite membrane was prepared on the outer surface of a porous α-Al_2O_3 support tube by the combination of the secondary growth of seed particles and the structure conversion of FAU-type zeolite [36–38]. The seed particles were prepared by mixing sodium hydroxide (FUJIFILM Wako, Tokyo, Japan), sodium aluminate (FUJIFILM Wako, Tokyo, Japan), a *N*,*N*,*N*-trimethyl-1-adamantammonium hydroxide solution (SDA, 25%, Sachem Asia, Osaka, Japan), and ultra-stable Y-type zeolite particles (HSZ-390HUA, Tosoh, Tokyo, Japan). The molar composition of the solution was 40 SiO_2:1 Al_2O_3:4 Na_2O:8 SDA:800 H_2O. The mixture was poured into a Teflon-lined stainless-steel autoclave, and a hydrothermal reaction was carried out at 433 K for 4 days. Solids were recovered by filtration, washed with distilled water, and dried overnight at 383 K to obtain seed particles. For the secondary growth, a synthesis solution was prepared by the same procedures as that for the seed particles, and the mixture was stirred at room temperature for 4 h. The molar composition of the mixture was 45 SiO_2:1 Al_2O_3:4.5 Na_2O:3.4 SDA:4500 H_2O. The α-Al_2O_3 tube was used as the support, and the properties were as follows: outer diameter = 2.0 mm; inside diameter = 1.5 mm; mean pore diameter = 0.3 μm; and porosity = 45%. The outer surface of the support tube was rubbed with the seed particles to implant seeds for nucleation, and the tube was added to the autoclave filled with 30 g of the synthesis solution. The autoclave was placed horizontally in an oven at 433 K for 20 h to form the polycrystalline high-silica CHA-type zeolite layer. After the autoclave was cooled to room temperature, the support tube was recovered, washed with distilled water, and dried at room temperature overnight. Finally, the tube was calcined in air at 773 K for 10 h to remove the SDA to obtain the high-silica CHA-type zeolite membrane.

The morphology was observed using a scanning electron microscope (SEM, TM-1000, Hitachi High-Technologies, Tokyo, Japan), and the composition was analyzed by an energy-dispersive X-ray (EDX) analyzer attached with the SEM. The crystal structure of the membrane was identified by X-ray diffraction (XRD, Smart-Lab, Rigaku, Tokyo, Japan).

2.2. Gas Permeation Test

Both the ends of the support tube were connected to stainless-steel tubes with silicon resin (TSE3976-B, Momentive, Tokyo, Japan), and the outer surfaces of resin were wrapped

with thermally shrinking tetrafluoroethylene and hexafluoropropylene copolymer (FEP) tubes (FEP-040, Junkosha, Osaka, Japan). The effective membrane area for permeation was 1.2 cm^2. The membrane was fixed to a permeation cell, as shown in Figure 1, and the cell was placed in an electric furnace [39]. Single-component H_2, CO_2, N_2, CH_4, n-C_4H_{10}, and SF_6, as well as binary mixtures of N_2–SF_6, CO_2–N_2, and CO_2–CH_4, were fed onto the outer surface of the membrane (feed side) at 100 mL min^{-1}, and either argon (for H_2) or helium (for the others) was introduced into the inside of the membrane (permeate side) at 10–50 mL min^{-1} as the sweep gas. The total pressures of the feed and permeate sides were kept at 300 and 101 kPa, respectively. In this study, the membrane was treated under N_2 flow at 473 K for 30 min to remove adsorbed water, and the test gas was fed onto the feed side. The pretreatment was carried out before each measurement. The gas composition was analyzed using a gas chromatograph with a thermal conductivity detector (Shimadzu GC-8A), and the gas flow rate was determined by a soap-film flowmeter. The permeance for component i, Q_i, was calculated using the following equation:

$$Q_i = \frac{N_p y_i}{S(P_{fi} - P_{pi})}, \quad (1)$$

where N_p is the molar flow rate of the outlet from the permeate side; S, the effective membrane area for permeation; y_i, the mole fraction of component i in the outlet gas of the permeate side; P_{fi}, the partial pressure of component i on the feed side; and P_{pi}, the partial pressure of component i on the permeate side. The selectivity was defined as the ratio of the permeances in this study.

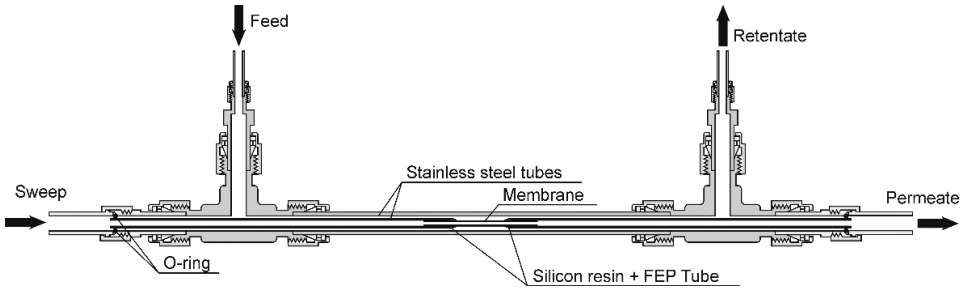

Figure 1. Schematic illustration of the gas permeation cell.

3. Results and discussion

3.1. Membrane Characterization

Figure 2 shows the SEM images of the CHA-type zeolite membrane. The outer surface of the porous support tube was covered with a polycrystalline layer (thickness ≈ 3 μm, Si/Al = 18). The XRD pattern of the membrane contained both the peaks of the support tube and seed particles, as shown in Figure 3. These are identical to those reported previously [36–38]. This suggests that the polycrystalline CHA-type zeolite layer could be formed on the porous α-Al_2O_3 tube with high reproducibility.

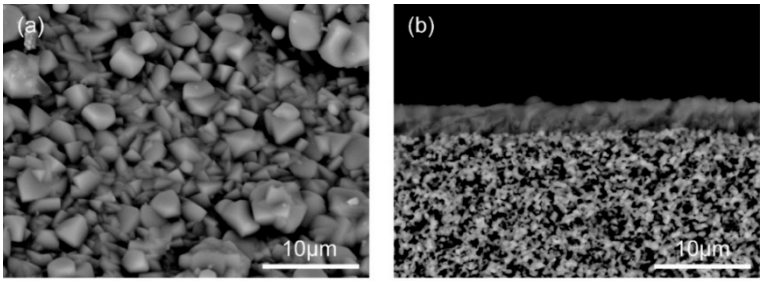

Figure 2. SEM images of (**a**) top surface and (**b**) fractured section of the high-silica CHA-type zeolite membrane.

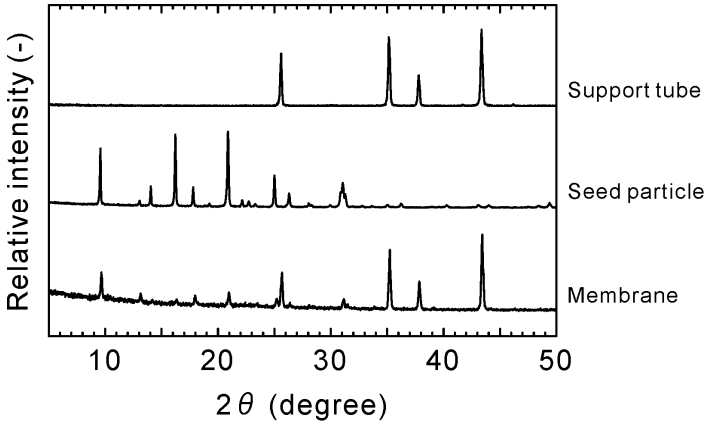

Figure 3. XRD patterns of the support tube, seed particles, and zeolite membrane.

3.2. Single-Component Gas Permeation

Figure 4 shows the influence of the kinetic diameter on the single-component gas permeance at 303 and 473 K. The permeance of CO_2 was 5.1×10^{-7} mol m^{-2} s^{-1} Pa^{-1} at 303 K. The permeance, except for H_2, decreased, with increase in the diameter, and that reached 4.1×10^{-11} mol m^{-2} s^{-1} Pa^{-1} for SF_6. The diameter of the crystallographic channel aperture of the CHA-type zeolite is 0.38 nm [23], and the molecular diameters of H_2, CO_2, N_2, CH_4, *n*-C_4H_{10}, and SF_6 are 0.289, 0.33, 0.364, 0.38, 0.43, and 0.55 nm, respectively [40]. Since H_2, CO_2, and N_2 molecules are smaller than the channel diameter, those molecules can penetrate into and diffuse within the zeolite channels. Although the molecular diameter of SF_6 is clearly larger than the channel sizes, SF_6 was detected on the permeate side of the membrane. The marginal permeance of SF_6 proposes that the membrane had intercrystalline boundaries. The unit cell of the high-silica CHA-type zeolite was shrunk by the air calcination, and the volume shrinkage degree was 0.6 vol % [37]. The small intercrystalline boundaries were produced by the unit cell shrinkage by the air calcination.

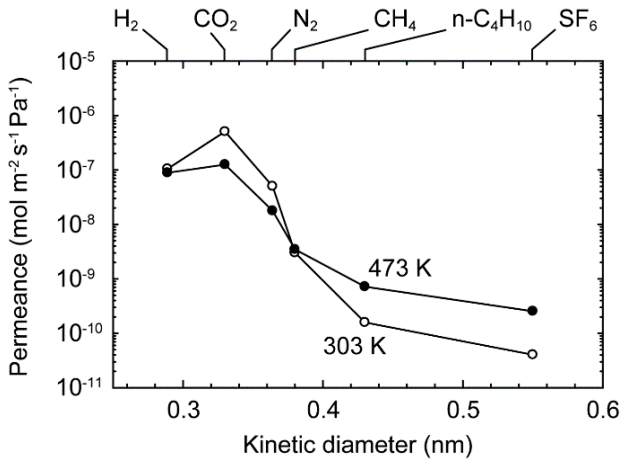

Figure 4. Influence of the kinetic diameters on the permeances of single-component gases at 303 and 473 K.

Moreover, the permeance of N_2 was 1.8×10^{-8} mol m^{-2} s^{-1} Pa^{-1} at 473 K. After nine times heating and cooling treatment for determination of the permeation properties of single-component gases and binary mixtures, the permeance was 1.7×10^{-8} mol m^{-2} s^{-1} Pa^{-1}. The identical permeances of N_2 indicates that the high-silica CHA-type zeolite membrane was stable for the thermal treatment.

Figure 5 shows the effect of temperature on the permeances of the single-component H_2, CO_2, N_2, CH_4, *n*-C_4H_{10}, and SF_6 at 303–473 K. The permeance of CO_2 was

5.1×10^{-7} mol m^{-2} s^{-1} Pa^{-1} at 303 K and decreased with temperature. As a result, it was 1.3×10^{-7} mol m^{-2} s^{-1} Pa^{-1} at 473 K. The permeances of H_2 and N_2 showed similar dependencies. Since these molecules are smaller than the channel diameter of the CHA-type zeolite, these molecules can adsorb on the zeolite channels. The adsorption amount decreased with temperature. Therefore, the permeances of H_2, CO_2, and N_2 were decreased with temperature by the reduction of the concentration difference between both the sides of the membrane.

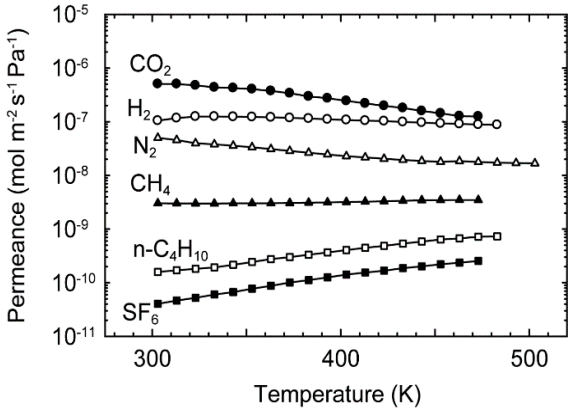

Figure 5. Effect of temperatures on permeances of single-component H_2, CO_2, N_2, CH_4, *n*-C_4H_{10}, and SF_6 at 303–473 K.

In contrast, for CH_4, *n*-C_4H_{10}, and SF_6, the diameters of which are identical or larger than the zeolite channels, the permeances increased with temperature. The effect of temperatures is described using the Arrhenius equation as follows:

$$Q_i = Q_i^* \exp\left(-\frac{E_p}{RT}\right), \quad (2)$$

where Q_i^* and E_p are the pre-exponential factor and activation energy for permeation, respectively. The pre-exponential factors and activation energies of single-component gas permeation are listed in Table 1. The activation energies for *n*-C_4H_{10} and SF_6 were higher than those of the other gases. It is well known that the difference in the diffusivities is important for the permeation through membranes [11–17]. The higher activation energies of *n*-C_4H_{10} and SF_6 suggest that it is difficult for these molecules to permeate through the intercrystalline boundaries. Therefore, the high-silica CHA-type zeolite membrane had small and minimal intercrystalline boundaries.

Table 1. Pre-exponential factors and activation energies for single-component gas permeation through the high-silica CHA-type zeolite membrane.

Gas	σ (nm)	Q_i^* (mol m^{-2} s^{-1} Pa^{-1})	E_p (kJ mol^{-1})
H_2	0.289	5.5×10^{-8}	−2.1
CO_2	0.33	9.5×10^{-9}	−10.6
N_2	0.364	2.7×10^{-9}	−7.5
CH_4	0.38	4.7×10^{-9}	1.2
n-C_4H_{10}	0.43	7.5×10^{-9}	11.3
SF_6	0.55	7.3×10^{-9}	13.2

As shown in Table 1, the order of the activation energies was $CO_2 < N_2 < CH_4 < SF_6$. This suggests that the CO_2/N_2, CO_2/CH_4, and N_2/SF_6 selectivities are higher at lower temperatures. The separation performances for these mixtures are examined in the next subsection.

3.3. Binary Mixture Gas Permeation

Figure 6 shows the permeances of N_2 and SF_6 for the equimolar mixture of them at 303–473 K. As same as for the single gas, the permeance of N_2 for the binary mixture decreased with temperature, while that of SF_6 showed the reverse dependency. Therefore, the N_2/SF_6 selectivity was the highest (=710) at 303 K. The permeance of SF_6 for the mixture was the same as that for single gas, and the permeance of N_2 for the mixture was also identical at temperatures higher than 363 K. However, below 363 K, the permeances of N_2 for the mixture was lower than that for the single gas. As a result, the N_2/SF_6 selectivity was 440 for the mixture. The lower N_2 permeances for the mixture was attributed to the weaker interaction of N_2 with the zeolite than SF_6. The interaction potential of individual molecules can be described using the Lennard–Jones 12-6 equation. The depths of interaction potential are 0.59 kJ mol^{-1} and 1.85 kJ mol^{-1} for N_2 and SF_6, respectively [41]. The deeper potential of SF_6 proposes that SF_6 molecules interact with zeolites more strongly than N_2. In addition, SF_6 molecules permeated through the boundaries, as discussed above. Therefore, N_2 molecules, permeated through the boundaries, were inhibited by the SF_6 molecules, and the permeance of N_2 became lower compared to the single gas.

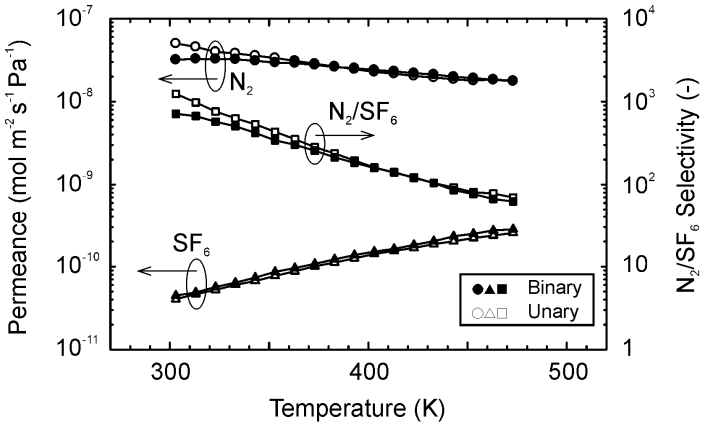

Figure 6. Gas permeation properties for the equimolar mixture of N_2 and SF_6 at 303–473 K.

Figure 7 shows the permeation properties of CO_2 and N_2 for the equimolar mixture of them at 303–473 K. Although the permeance of N_2 became the maximum at 343 K for the mixture, that of CO_2 decreased with temperature. The CO_2/N_2 selectivity for the mixture was the highest at 303 K (=25) and decreased with temperature. As a result, the selectivity became only 9 at 473 K.

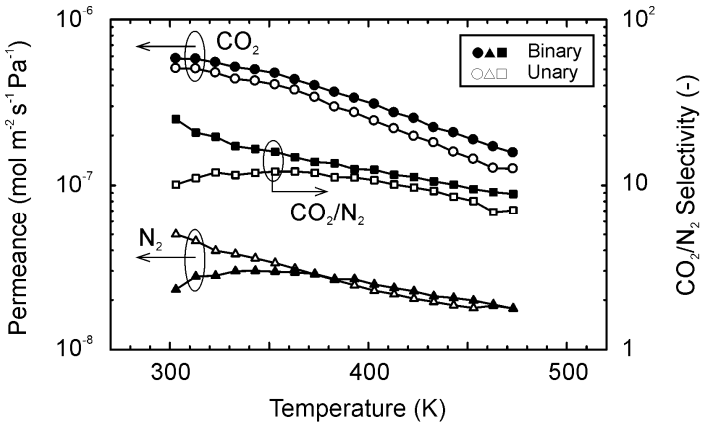

Figure 7. Gas permeation properties for the equimolar mixture of CO_2 and N_2 at 303–473 K.

Compared to the single gas, the temperature dependency of CO_2 for the mixture was similar, although the permeance for the mixture was slightly higher at all temperatures.

The permeance of N_2 was almost the same that for the single gas at higher temperatures than 373 K, while it was lower below 363 K. These are typical permeation properties when molecules are transferred and separated by the preferential adsorption of CO_2. Similar properties were also observed for the CO_2–N_2 separation using FAU-type zeolite membranes [15,16]. Morooka and coworkers explained the permeation properties by the preferential CO_2 adsorption and the overtaking N_2 by CO_2 [15].

Figure 8 shows the effect of temperatures on the permeation properties of CO_2 and CH_4 for the equimolar mixture of them. The permeances of CO_2 and CH_4 for the mixture were 5.3×10^{-7} and 2.2×10^{-9} mol m^{-2} s^{-1} Pa^{-1} at 303 K, respectively. The CO_2/CH_4 selectivity was 240 for the mixture. The permeance of CO_2 decreased with temperature, although that of CH_4 showed the reverse dependency. As a result, the CO_2/CH_4 selectivity reduced to 43 at 473 K. Comparing to the single gases, the permeances of CO_2 and CH_4 for the mixture were almost identical. The permeation properties cannot be explained by only the preferential CO_2 adsorption, as discussed in Figure 7. Since the molecular size of CH_4 is similar to the channel diameter of the CHA-type zeolite, the diffusion of CH_4 within the zeolite channel was slower than N_2, as show in Figure 4. It is known that the *i*-C_4H_{10} molecules hinder the diffusion of *n*-C_4H_{10} for the separation of butane isomers using MFI-type zeolite membranes [39]. The CH_4 molecules within the zeolite channels may hinder the diffusion of CO_2 molecules.

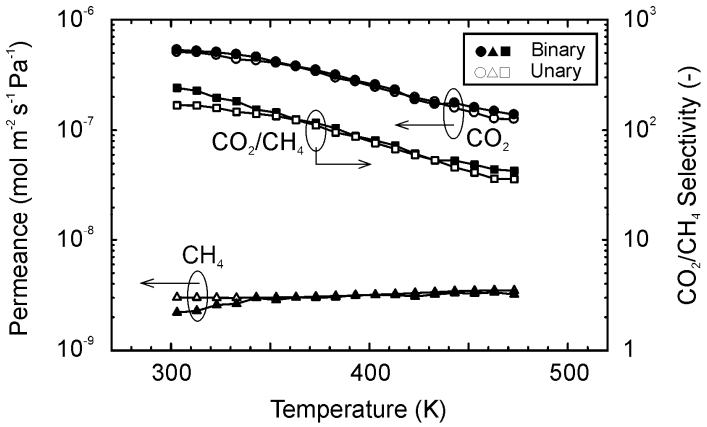

Figure 8. Gas permeation properties for the equimolar mixture of CO_2 and CH_4 at 303–473 K.

The influence of the CO_2 concentration in the feed mixture was determined to check the interaction between CO_2 and CH_4 molecules during the permeation. Figure 9 shows the influences of the CO_2 concentration in the feed mixtures on the permeation properties of CO_2 and CH_4 for binary mixtures of them at 303 K. If CH_4 inhibits the permeation of CO_2, the permeance of CO_2 would be reduced at the dilute CO_2 concentration. However, the permeances of CO_2 and CH_4 were independent of the CO_2 concentration in the feed mixture, and the selectivity was almost constant at 200–260. The constant permeances of CO_2 and CH_4 propose that the CO_2 and CH_4 molecules did not interact each other during the membrane permeation. Therefore, it is considered that CO_2 and CH_4 molecules diffuse in the different passes, such as zeolite micropores and inter-crystalline boundaries.

Figure 10 compares the CO_2 separation performance to previous reports [25,27,28,32,34,42,43]. The CO_2 permeance and selectivity of our membrane were relatively high for CO_2–CH_4 mixtures, and the performances could be plotted on the trade-off line of SAPO-34, CHA-, and AEI-type zeolite membranes [27,28,32–34]. It is considered that the similar CO_2 separation performances of the membranes are attributed to the similar crystal structures [44]. Although the DDR-type zeolite membrane showed extremely high CO_2 selectivity below 300 K, the selectivity at temperature higher than 300 K was almost the same as those of CHA- and AEI-type zeolite membranes [25]. The CO_2 selectivities of the FAU-type zeolite membranes were lower compared to those membranes [42]. On the contrary, the FAU-type zeolite membranes showed higher CO_2 permeance and selectivity

for CO_2–N_2 mixtures [42,43]. The selectivity of our membrane was an order of magnitude lower than those of the FAU-type zeolite membranes and comparable to those of the DDR-type zeolite membrane around 300 K. The Si/Al ratio of the DDR- and CHA-type zeolite membranes were more than 15, and the amount of the counter-cation was much less. In contrast, the FAU-type zeolite membrane contained many cations because of low Si/Al ratio (Si/Al < 2). These propose that the effect of molecular sieving such as the DDR-, CHA-, and AEI-type zeolite membranes is effective for the CO_2 separation from CH_4, while the selective adsorption of CO_2 is necessary for CO_2–N_2 mixtures.

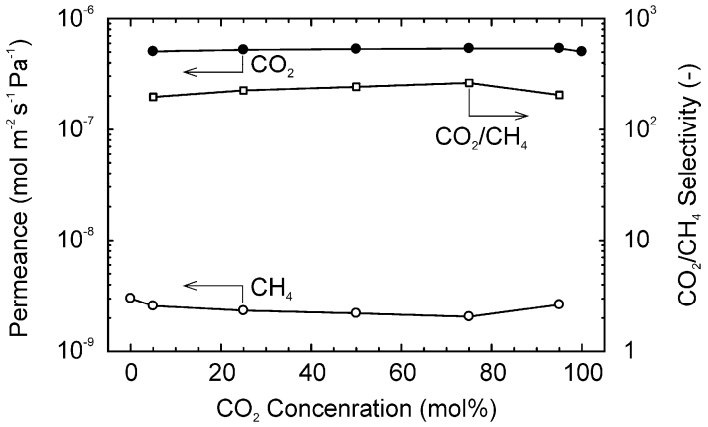

Figure 9. Influence of the feed gas composition on the gas permeation properties for the binary mixtures of CO_2 and CH_4 303 K.

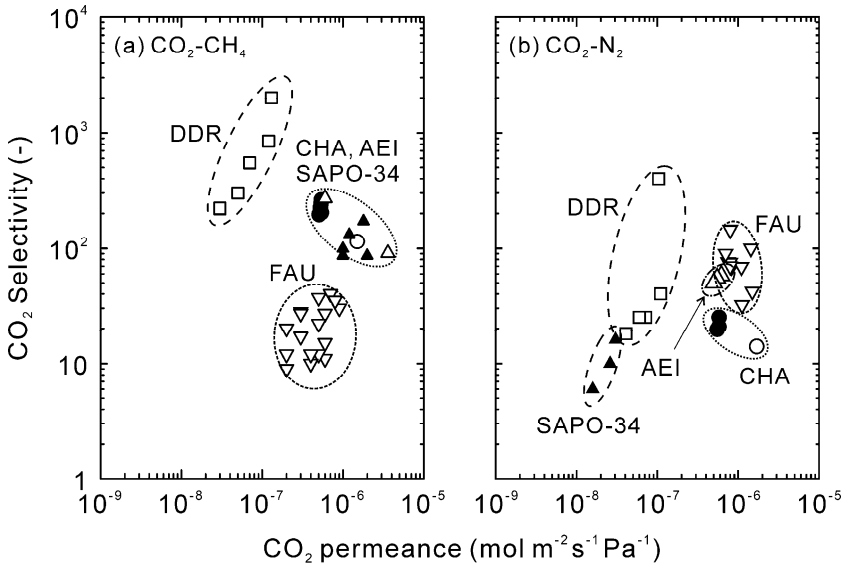

Figure 10. Comparison of the CO_2 separation performance to previous reports [25,27,28,32,34,42,43].

4. Conclusions

The polycrystalline CHA-type zeolite layer with Si/Al = 18 was formed on the porous α-Al_2O_3 tube in this study, and the gas permeation properties were determined using single-component H_2, CO_2, N_2, CH_4, n-C_4H_{10}, and SF_6 at 303–473 K. The permeance was 5.1 × 10^{-7} mol m^{-2} s^{-1} Pa^{-1} for CO_2 at 303 K and the permeance reduced with increasing the molecular size. Moreover, the permeances of H_2, CO_2, and N_2 decreased with temperature, while those of CH_4, n-C_4H_{10}, and SF_6 showed reverse trends. The gas separation tests were also carried out using binary mixtures of N_2-SF_6, CO_2-N_2, and CO_2-CH_4. The membrane showed the high separation performance for the mixtures, and the N_2/SF_6, CO_2/N_2, and CO_2/CH_4 selectivities were 710, 25, and 240, respectively.

Author Contributions: Conceptualization, Y.H.; methodology, Y.H.; validation, A.I. and Y.H.; formal analysis, Y.H.; investigation, C.A. and M.N.; resources, Y.H.; data curation, Y.H.; writing—original draft preparation, Y.H.; writing—review and editing, Y.H. and A.I.; visualization, Y.H.; supervision, Y.H.; project administration, Y.H.; funding acquisition, Y.H. All authors have read and agreed to the published version of the manuscript.

Funding: This research received no external funding.

Institutional Review Board Statement: Not applicable.

Informed Consent Statement: Not applicable.

Data Availability Statement: Not applicable.

Conflicts of Interest: The authors declare no conflict of interest.

References

1. Geus, E.R.; den Exter, M.J.; van Bekkum, H. Synthesis and characterization of zeolite (MFI) membranes on porous ceramic supports. *J. Chem. Soc. Faraday Trans.* **1992**, *88*, 3101–3109. [CrossRef]
2. Sano, T.; Yanagishita, H.; Kiyozumi, Y.; Mizukami, F.; Haraya, K. Separation of ethanol/water mixture by silicalite membrane on pervaporation. *J. Membr. Sci.* **1994**, *95*, 221–228. [CrossRef]
3. Kusakabe, K.; Yoneshige, S.; Murata, A.; Morooka, S. Morphology and gas permeance of ZSM-5-type zeolite membrane formed on a porous α-alumina support tube. *J. Membr. Sci.* **1996**, *116*, 39–46. [CrossRef]
4. Lai, R.; Gavalas, G.R. ZSM-5 membrane synthesis with organic-free mixtures. *Micropor. Mesopor. Mater.* **2000**, *38*, 239–245. [CrossRef]
5. Gump, C.J.; Lin, X.; Falconer, J.L.; Noble, R.D. Experimental configuration and adsorption effects on the permeation properties of C4 isomers through ZSM-5 zeolite membranes. *J. Membr. Sci.* **2000**, *173*, 35–52. [CrossRef]
6. Pan, M.; Lin, Y.S. Template-free secondary growth synthesis of MFI type zeolite membranes. *Micropor. Mesopor. Mater.* **2001**, *43*, 319–327. [CrossRef]
7. Takata, Y.; Tsuru, T.; Yoshioka, T.; Asaeda, M. Gas permeation properties of MFI zeolite membranes prepared by the secondary growth of colloidal silicalite and application to the methylation of toluene. *Miropor. Mesopor. Mater.* **2002**, *54*, 257–268. [CrossRef]
8. Hedlund, J.; Jareman, F.; Bons, A.J.; Anthonis, M. A masking technique for high quality MFI membranes. *J. Membr. Sci.* **2003**, *222*, 163–179. [CrossRef]
9. Li, G.; Kikuchi, E.; Matsukata, M. ZSM-5 zeolite membranes prepared from a clear template-free solution. *Micropor. Mesopor. Mater.* **2003**, *60*, 225–235. [CrossRef]
10. Bernal, M.P.; Coronas, J.; Menéndez, M.; Santamaria, J. On the effect of morphological features on the properties of MFI zeolite membranes. *Microporous Mesoporous Mater.* **2003**, *60*, 99–110. [CrossRef]
11. Kapteijn, F.; Bakker, W.J.W.; Zheng, G.; Poppe, J.; Moulijn, J.A. Permeation and separation of light hydrocarbons through a silicalite-1 membrane Application of the generalized Maxwell-Stefan equations. *Chem. Eng. J.* **1995**, *57*, 145–153.
12. Bakker, W.J.W.; van den Broeke, L.J.P.; Kapteijn, F.; Moulijn, J.A. Temperature dependence of one-component permeation through a silicalite-1 membrane. *AIChE J.* **1997**, *43*, 2203–2214. [CrossRef]
13. Van de Graaf, J.M.; Kapteijn, F.; Moulijn, J.A. Modeling permeation of binary mixtures through zeolite membranes. *AIChE J.* **1999**, *45*, 497–511. [CrossRef]
14. Van den Broeke, L.J.P.; Bakker, W.J.W.; Kapteijn, F.; Moulijn, J.A. Binary permeation through a silicalite-1 membrane. *AIChE J.* **1999**, *45*, 976–985. [CrossRef]
15. Kusakabe, K.; Kuroda, T.; Uchino, K.; Hasegawa, Y.; Morooka, S. Gas permeation properties of ion-exchanged faujasite-type zeolite membranes. *AIChE J.* **1999**, *45*, 1220–1226. [CrossRef]
16. Hasegawa, Y.; Kusakabe, K.; Morooka, S. Effect of temperature on the gas permeation properties of NaY-type zeolite formed on the inner surface of a porous support tube. *Chem. Eng. Sci.* **2001**, *56*, 4273–4281. [CrossRef]
17. Carreon, M.A. Porous crystals as membranes. *Science* **2020**, *367*, 624–625. [CrossRef]
18. Morigami, Y.; Kondo, M.; Abe, J.; Kita, H.; Okamoto, K. The first large-scale pervaporation plant using tubular-type module with zeolite NaA membrane. *Sep. Purif. Technol.* **2001**, *25*, 251–260. [CrossRef]
19. Sato, K.; Aoki, K.; Sugimoto, K.; Izumi, K.; Inoue, S.; Saito, J.; Ikeda, S.; Nakane, T. Dehydration performance of commercial LTA zeolite membranes and application to fuel cell grade bio-ethanol production by hybrid distillation/vapor permeation process. *Microporous Mesoporous Mater.* **2008**, *115*, 184–188. [CrossRef]
20. Tomita, T.; Nakayama, K.; Sakai, H. Gas separation characteristics of DDR type zeolite membrane. *Microporous Mesoporous Mater.* **2004**, *68*, 71–75. [CrossRef]
21. Zeng, W.; Li, B.; Li, H.; Jin, H.; Li, Y. Mass produced NaA zeolite membranes for pervaporative recycling of spent N-methy-2-Pyrrolidone in the manufacturing process for lithium-ion battery. *Sep. Purif. Technol.* **2019**, *228*, 115741. [CrossRef]
22. Okazaki, J.; Hasegawa, H.; Chikamatsu, N.; Yamaji, K.; Shimizu, K.; Niino, M. DDR-type zeolite membrane: A novel CO_2 separation technology for enhanced oil recovery. *Sep. Purif. Technol.* **2019**, *219*, 200–205. [CrossRef]

23. Baerlocher, C.; McCusker, L.B.; Olson, D.H. *Atlas of Zeolite Framework Types*, 6th ed.; Elsevier: Amsterdam, The Netherlands, 2007.
24. Hasegawa, Y.; Abe, C.; Nishioka, M.; Sato, K.; Nagase, T.; Hanaoka, T. Influence of synthesis gel composition on morphology, composition, and dehydration performance of CHA-type zeolite membranes. *J. Membr. Sci.* **2010**, *363*, 256–264. [CrossRef]
25. Van den Bergh, J.; Zhu, W.; Gascon, J.; Moulijn, J.A.; Kapteijn, F. Separation and permeation characteristics of a DD3R zeolite membrane. *J. Membr. Sci.* **2008**, *316*, 35–45. [CrossRef]
26. Poshusta, J.C.; Tuan, V.A.; Falconer, J.L.; Noble, R.D. Synthesis and permeation properties of SAPO-34 tubular membranes. *Ind. Eng. Chem. Res.* **1998**, *37*, 3924–3929. [CrossRef]
27. Poshusta, J.C.; Tuan, V.A.; Pape, E.A.; Noble, R.D.; Falconer, J.L. Separation of light gas mixtures using SAPO-34 membranes. *AIChE J.* **2000**, *46*, 779–789. [CrossRef]
28. Crreon, M.A.; Li, S.; Falconer, J.L.; Noble, R.D. Alumina-supported SAPO-34 membranes for CO_2/CH_4 separation. *J. Am. Chem. Soc.* **2008**, *130*, 5412–5413. [CrossRef]
29. Feng, X.; Zong, Z.; Elsaidi, S.K.; Jasinski, J.B.; Krishna, R.; Thallapally, P.K.; Carreon, M.A. Kr/Xe separation over a chabazite zeolite membrane. *J. Am. Chem. Soc.* **2016**, *138*, 9791–9794. [CrossRef]
30. Zong, Z.; Feng, X.; Huang, Y.; Song, Z.; Zhou, R.; Zhou, S.J.; Carreon, M.A.; Yu, M.; Li, S. Highly permeable N_2/CH_4 separation SAPO-34 membranes synthesized by diluted gels and increased crystallization temperature. *Microporous Mesoporous Mater.* **2016**, *224*, 36–42. [CrossRef]
31. Sato, K.; Sugimoto, K.; Shimotsuma, N.; Kiuchi, T.; Kyotani, T.; Kurata, T. Development of practically available up-scaled sigh-silica CHA-type zeolite membrane for industrial purpose in dehydration of *N*-methyl pyrrolidone solution. *J. Membr. Sci.* **2012**, *409–410*, 82–95. [CrossRef]
32. Imasaka, S.; Itakura, M.; Yano, K.; Fujita, S.; Okada, M.; Hasegawa, Y.; Abe, C.; Araki, S.; Yamamoto, H. Rapid preparation of high-silica CHA-type zeolite membranes and their separation properties. *Sep. Purif. Technol.* **2018**, *199*, 298–303. [CrossRef]
33. Wang, B.; Hu, N.; Wang, H.; Zheng, Y.; Zhou, R. Improved AlPO-18 membranes for light gas separation. *J. Mater. Chem. A* **2015**, *3*, 12205–12212. [CrossRef]
34. Wang, B.; Gao, F.; Zhang, F.; Xing, W.; Zhou, R. Highly permeable and oriented AlPO-18 membrane prepared using directly synthesized nanosheets for CO_2/CH_4 separation. *J. Mater. Chem. A* **2019**, *7*, 13164–13172. [CrossRef]
35. Zhan, T.; Wu, T.; Shi, Y.; Chen, X.; Li, Y.; Zhu, M.; Kumakiri, I.; Chen, X.; Kita, H. Influence of synthesis parameters on the preparation of AlPO-18 membranes by single DIPEA for CO_2/CH_4 separation. *J. Membr. Sci.* **2020**, *601*, 117853. [CrossRef]
36. Hasegawa, Y.; Abe, C.; Sato, K.; Sano, T. Preparation of high-silica chabazite membrane. *Maku(Membrane)* **2014**, *39*, 56–60. [CrossRef]
37. Hasegawa, Y.; Abe, C.; Ikeda, T.; Sato, K.; Imasaka, S.; Itakura, M.; Yano, K. Influence of the synthesis parameters on the morphology and dehydration performance of high-silica chabazite membranes. *Adv. Porous Mater.* **2016**, *4*, 134–143. [CrossRef]
38. Hasegawa, Y.; Abe, C.; Ikeda, A. Pervaporative dehydration of organic solvents using high-silica CHA-type zeolite membrane. *Membranes* **2021**, *11*, 229. [CrossRef]
39. Hasegawa, Y.; Ikeda, T.; Nagase, T.; Kiyozumi, Y.; Hanaoka, T.; Mizukami, F. Preparation and characterization of silicalite-1 membranes prepared by secondary growth of seed with different crystal sizes. *J. Membr. Sci.* **2006**, *280*, 397–405. [CrossRef]
40. Breck, D.W. *Zeolite Molecular Sieves*; Wiley: New York, NY, USA, 1974.
41. Poling, B.E.; Prausnitz, J.M.; O'Connell, J.P. *The Properties of Gases and Liquids*, 5th ed.; McGraw-Hill: New York, NY, USA, 2001.
42. Hasegawa, Y.; Tanaka, T.; Watanabe, K.; Jeong, B.H.; Kusakabe, K.; Morooka, S. Separation of CO_2-CH_4 and CO_2-N_2 systems using ion-exchanged FAU-type zeolite membranes with different Si/Al ratios. *Korean J. Chem. Eng.* **2002**, *19*, 309–313. [CrossRef]
43. Hasegawa, Y.; Watanake, K.; Kusakabe, K.; Morooka, S. Influence of alkali cations on permeation properties of Y-type zeolite membranes. *J. Membr. Sci.* **2002**, *208*, 415–418. [CrossRef]
44. Hasegawa, Y.; Abe, C.; Ikeda, T.; Sato, K. Influence of change in the unit cell parameters on permeation properties of AEI-type zeolite membrane. *J. Membr. Sci.* **2016**, *499*, 538–543. [CrossRef]